Chapter 4

Structural dynamic response reconstruction

The dynamic forces exerted on the cutting tool during the machining process have to be acquired in order to perform a mathematical simulation of the cutting process. The forces exerted on to the tool tip of a lathe during the machining operation are traditionally measured with a dynamometer. However, the introduction of a load sell will alter the dynamic properties of the system considered in chapter 3. The problem of accurate dynamic force measurement is experienced in a number of structural research fields. In most cases the structural response is measured under operational conditions and an inverse model is used to calculate the input forces from the measured response. However, it is not that simple to obtain an inverse model. Most of the dynamic models of structures in practice suffer from ill conditioning when the inverse of the model is calculated. Therefore, special techniques have to be implemented to obtain the dynamic inverse model and input forces.

4.1 Structural dynamic response reconstruction

The concept of dynamic force estimation from the measured structural response is referred to as Structural Dynamic Response Reconstruction (SDRR). The techniques of SDRR are widely used in the service load industry for the durability testing of structures. The work of Raath [43] presents a thorough overview of the concepts and issues involved in the SDRR process.

Raath [43] proposed a system identification approach that is used to construct an inverse model of the structure from measured process data. The approach produces a stable inverse model which can be used to estimate the input forces. Certain changes were incorporated in the implementation of the technique to accommodate the model structure of the tool holder and shank in the force calculation process.

4.2 Response measurement

The objective was set to determine the horizontal and vertical forces on the tool tip. Therefore the response of the tool holder was measured in the vertical and horizontal directions, to obtain a reference response to each cutting force. The measurements were taken near the tip of the tool during a machining operation. Figure 4.1 indicates the measurement positions on the holder. Further details on the response measurements and machining conditions are presented in tables 4.1(a) and (b).

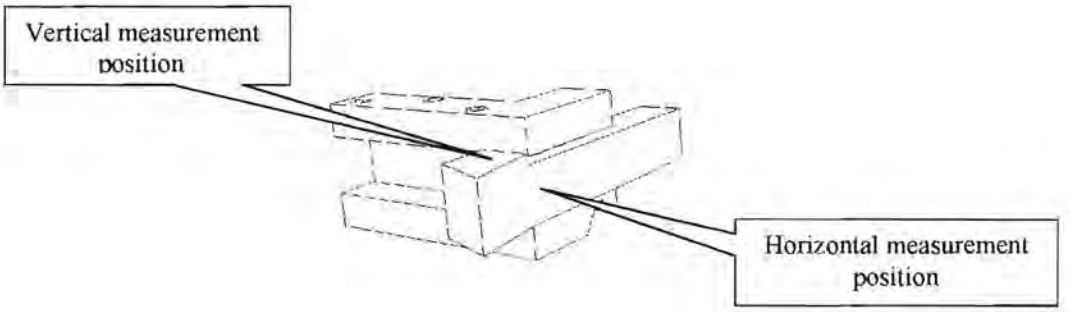

Figure 4.1 *Response measurement positions*

Table 4.1 (a) Details of the machining operation

Shaft length between the tailstock and the chuck	250 mm
Shaft diameter	40 mm
Shaft material	EN 8
Feed rate	0.2 mm/rev
Rotational speed	840 rpm
Cut depth	1.5 mm

Table 4.1 (b) Instrumentation used in the response measurement

Item number	Item	Model
1	DSP Siglab signal processor	20-42
2	Notebook computer	Intel 486 DX2-66
3	PCB miniature high frequency accelerometer	353B17
4	PCB battery powered signal conditioner	480E09

4.3.1 System identification overview

System identification techniques are used to build dynamic process models. The techniques construct transfer functions from measured input and output time signals. Only discrete time points are considered since the signals are recorded at discrete time instances. A schematic representation of the system is shown in figure 4.2.

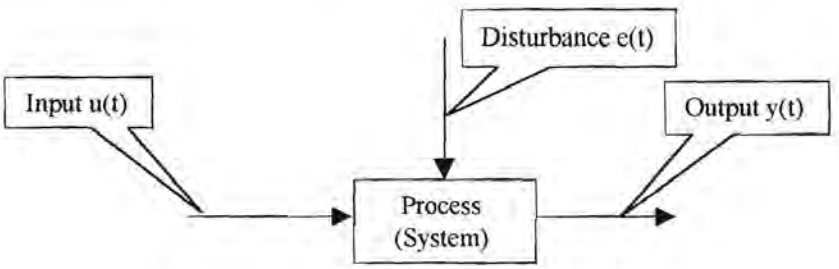

Figure 4.2 *System model*

A system identification model is described by a difference equation that relates the response of the system to the input of the system through a combination of past input and output instances. Several of these difference equations exist with their own unique properties, which accommodate the modelling of process noise and non-linearity.

The Auto Regressive model with eXternal input (ARX) is a linear model formulation known for its simplicity and ease of use. Raath proposed a convenient procedure to estimate a stable inverse model of a system that becomes ill conditioned when attempting to invert its dynamic model. The inverse ARX model facilitates the dynamic force calculation. The difference equation of a Single Input Single Output (SISO) ARX model is presented in equation 4.1.

$$\begin{aligned} &y(t)+a_1 y(t-T)+\ldots+a_{na} y(t-na\times T)= \\ &b_1 u(t-nk\times T)+\ldots+b_{nb} u(t-nk\times T-nb\times T+1)+e(t) \end{aligned} \tag{4.1}$$

with:

$u(t)$: System input
$y(t)$: System response
$e(t)$: Innovation term
a : Input parameter
b : Output parameter
na : Number of input parameters
nb : Number of output parameters
T : Sampling interval
nk : Time delay

The difference equation of the ARX model can be rewritten to produce the output at time t as a linear combination of past inputs and outputs.

$$\begin{aligned} y(t) = &-a_1 y(t-T)-\ldots-a_{na} y(t-na\times T)+ \\ &b_1 u(t-nk\times T)+\ldots+b_{nb} u(t-nk\times T-nb\times T+1)+e(t) \end{aligned} \tag{4.2}$$

The system identification process entails the estimation of parameter values, the number of parameters required and a time delay. The time delay refers to the time that passes until a change in the input influences the output. The parameters of the difference equation are estimated by a least squares estimate procedure. The innovation term represents the part of the output that cannot be determined from past and present data. Equation 4.3 represents the innovation term.

$$e(t) = y(t) - \hat{y}(t)$$
$$e(t) = y(t) - a_1 y(t-T) - \ldots - a_{na} y(t - na \times T) + b_1 u(t - nk \times T) + \ldots + b_{nb} u(t - nk \times T - nb \times T + 1) \tag{4.3}$$

with:

$\hat{y}(t)$: Output estimate

The least squares parameter estimation procedure employs a loss function, which is minimised to obtain a set of equations. The loss function is presented in equation 4.4.

$$V_N = \frac{1}{N} \sum_{t=1}^{N} e^2(t) \tag{4.4}$$

with:

N : Number of sampled time intervals

The advantage of the least squares parameter estimation is the fact that the quadratic loss function can be minimised analytically with respect to the parameters as indicated by equation 4.5.

$$\frac{\partial V_n}{\partial a_1} = \ldots = \frac{\partial V_n}{\partial a_{na}} = \frac{\partial V_n}{\partial b_1} = \ldots = \frac{\partial V_n}{\partial b_{nb}} = 0 \tag{4.5}$$

The partial differentiation of the loss function with respect to the various parameters results in a number of equations that are solved simultaneously to obtain the various parameter values. The number of parameters and time delay required to simulate the system is obtained though inspection.

4.3.2 Reverse inverse model

A forward ARX model is estimated from the measured input output data of a system. The input and output data signals are swapped in the estimation of the inverse model. However the inverse model violates the concept of causality, meaning that the system is required to respond to input which has not been induced. Raath [43] proposed the estimation of a reverse inverse model that does not violate the concept of causality. Sufficient proof is given by Raath [43] to validate the reverse inverse technique.

The reverse inverse model estimation requires that the input output data signals are swapped and reversed in order. The reverse inverse technique that Raath [43] proposed is only valid on Multiple Input Single Output (MISO) models. A number of MISO models are estimated to accommodate Multiple Input Multiple Output models (MIMO).

4.3.3 Force computation with the reverse inverse ARX model technique

The first step in the force computation process is to obtain input output data from the forward model. A white noise signal is used to excite the forward model in order to obtain model response data. The input output data is filtered with a high pass filter to remove trends from the data. The data is filtered with a low pass filter to omit the higher frequency data where no response is observed in the structural response measurements.

The order of the data is reversed and the input output signals are swapped to estimate the reverse inverse ARX model parameters. Two thirds of the data is used to estimate the model. The remaining third of the response data is used to calculate the known force input with the reverse inverse ARX model. The reverse inverse ARX model is validated by the correlation between the identification force and the force calculated with the reverse inverse ARX model.

The forces calculated for a MIMO system are dependent on each other. A number of MISO reverse inverse ARX models are estimated to approximate the MIMO model. Each MISO model is used to calculate a force input of the forward model. The output of the various reverse inverse MISO models are fed back to the model inputs in a finite difference feedback loop to accommodate the influence of the various calculated forces on each other. Figure 4.3 shows a flow diagram of the finite difference feedback loop for a reverse inverse ARX model with two inputs and two outputs.

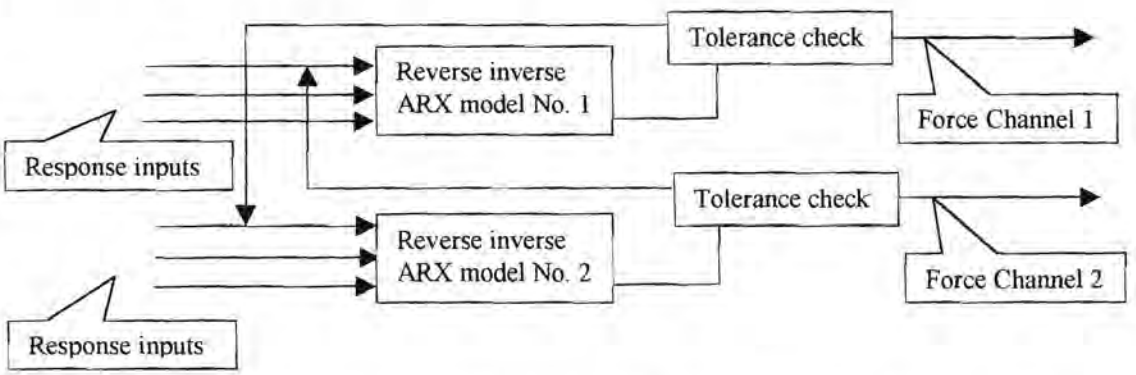

Figure 4.3 *MIMO reverse inverse ARX model with finite difference feedback loop*

Random force signals are initially used as inputs to the system to simulate the force input signals of the forward model. The force signals obtained from the previous simulation are used as the force input signals to the next simulation. The simulation loop is continued until the difference between the force signals used as the force inputs to the simulation and the force signals obtained from the simulation is less than a specified tolerance.

The number of input and output parameters as well as the time delay needs to be specified by the user in the model estimation process. Raath [43] states that the number of input parameters should equal the number of output parameters of the model. The number of parameters is referred to as the model order. No time delay is specified since most structural systems react fast enough to the system input.

An iteration process may improve the accuracy of the force estimation. The initial force estimate is used to excite the forward model in order to obtain the response to the initial force estimate. The difference between the response obtained from the simulation and the operational response is calculated and is used as an input to the reverse inverse model to compute the error in the force estimate. The error in the force is added to the previous force estimate and is used as an input to the forward simulation. The iteration response is compared to the measured response to determine whether the error in the response has diverged. The procedure is repeated as long as the error between the measured and iteration response converges. The error will diverge in certain cases. A diagram of the process is shown in figure 4.4.

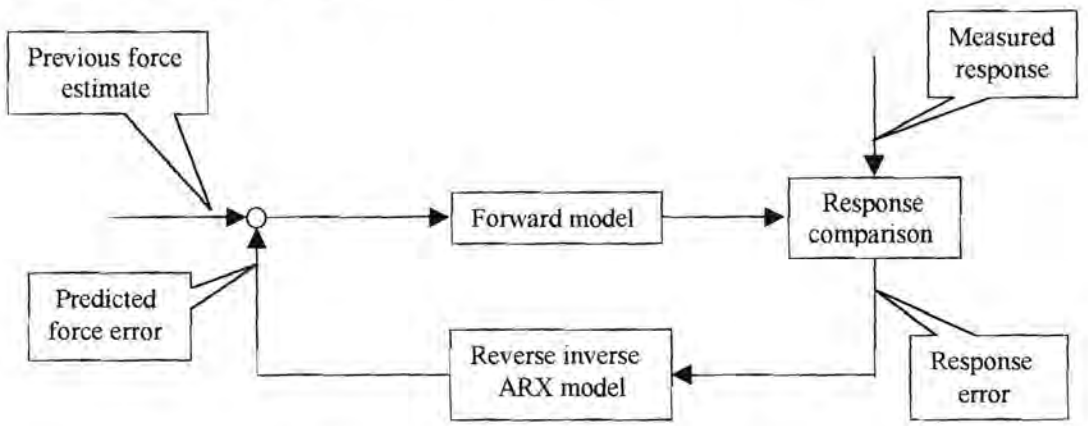

Figure 4.4 *Force iteration diagram*

4.3.4 Evaluation criteria

The error between the measured and calculated response signals is evaluated with a standard statistic correlation. However a more sensitive parameter was required to evaluate the iteration or simulation error. Therefore a new parameter or expression, in terms of the Root Mean Square (RMS) amplitude values of the signals, were defined to evaluate the results. The expression is defined in equation 4.6.

$$Simulation\ Error\ [\%] = \frac{MRA_{RMS} - CRA_{RMS}}{MRA_{RMS}} \times 100 \tag{4.6}$$

with:

MRA_{RMS} : RMS value of the Measured Response signal Amplitude

CRA_{RMS} : RMS value of the Calculated Response signal Amplitude

The reverse inverse ARX model is validated by a comparison between a white noise reference force and a calculated force as explained in section 4.3.3. Therefore equation 4.6 is redefined as equation 4.7 to accommodate the model validation process .

$$Model\ Error\ [\%] = \frac{RFA_{RMS} - CFA_{RMS}}{RFA_{RMS}} \times 100 \tag{4.7}$$

with:

RFA_{RMS} : RMS value of the Reference Force signal Amplitude

CFA_{RMS} : RMS value of the Calculated Force signal Amplitude

4.3.5 Force computation results with the reverse inverse ARX technique

A number of reverse inverse ARX models were estimated and validated to determine the optimal model order. The model order values were selected between one and eight. Figure 4.5 reveals the validation results of the various model order simulations. The combined model error is the sum of the vertical and horizontal model error. The optimal model was obtained at an order of four.

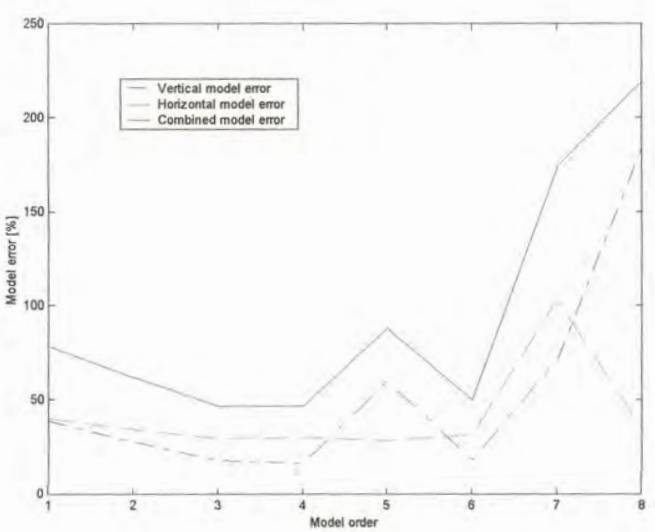

Figure 4.5 *Model order simulation results*

The simulation iteration results for the various models in terms of the simulation error is presented in figures 4.6 (a) and (b). The simulation error is defined by equation 4.6. The figures indicate that the iteration process was unsuccessful since the simulation error diverged in the simulation process. The more accurate the model the less the divergence.

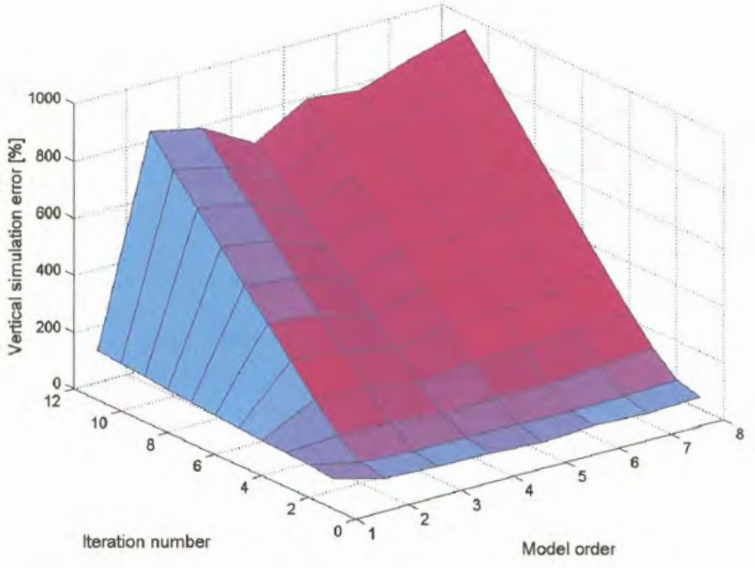

Figure 4.6 (a) *Vertical simulation error*

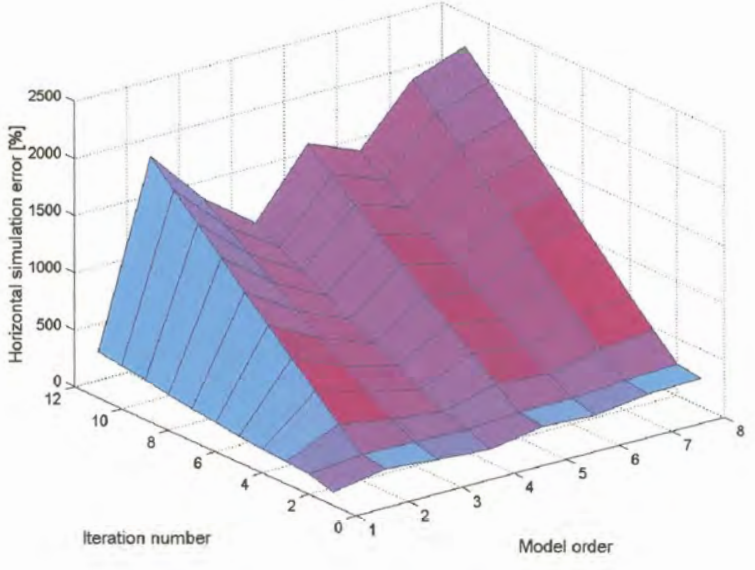

Figure 4.6 (b) *Horizontal simulation error*

Figures 4.7 (a) and (b) indicate the correlation coefficients for the simulations in figures 4.6 (a) and (b). The correlation coefficient does not indicate the reduction in the accuracy of the response reconstruction as well as the simulation error criteria during the simulation process.

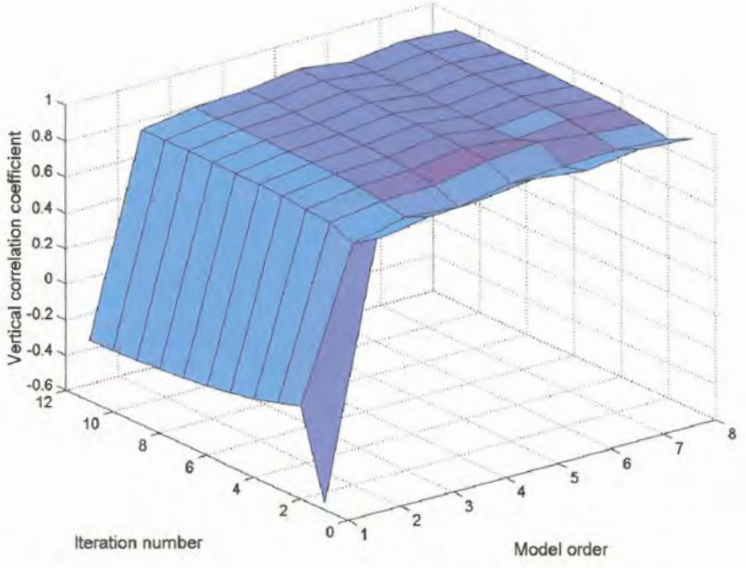

Figure 4.7(a) *Vertical correlation coefficient*

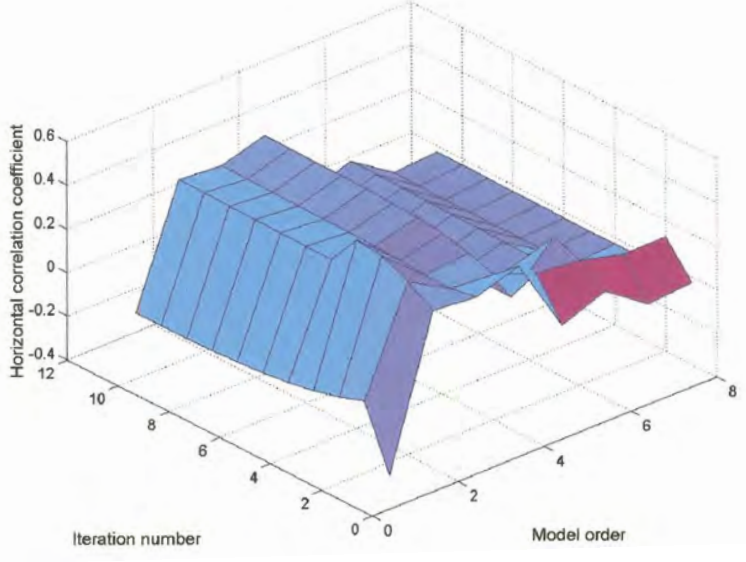

Figure 4.7 (b) *Horizontal correlation coefficient*

The optimum results of the SDRR process on the tool holder and shank is indicated in table 4.2.

Table 4.2 Optimum results of the SDRR process

Direction	Simulation Error [%]	Correlation coefficient [%]
Vertical	42.62	90.72
Horizontal	123.35	36.95

The optimum reconstructed response is compared to the measured response data in figures 4.8 (a) to (d). The time signals and Fast Fourier Transforms (FFT) of the signals are presented.

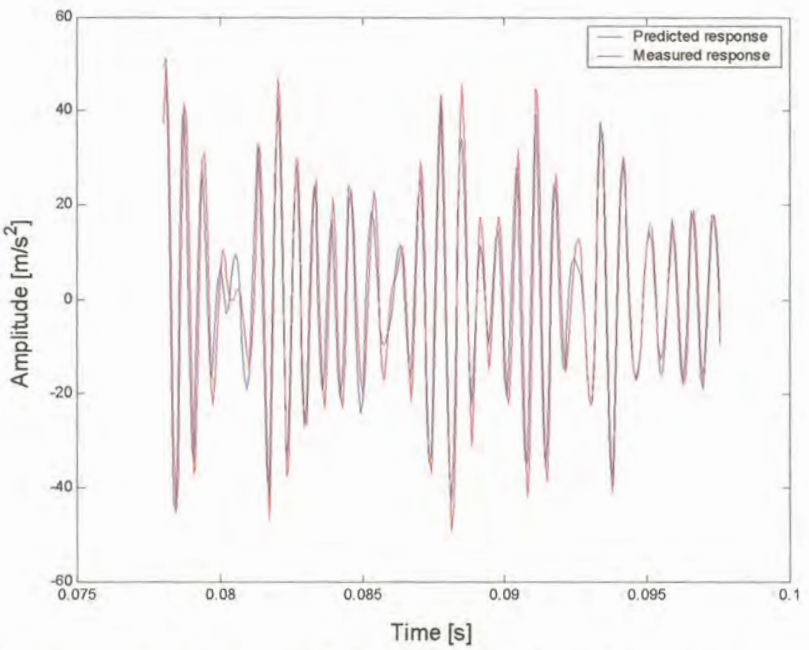

Figure 4.8 (a) *Comparison between the measured and predicted response in the vertical direction*

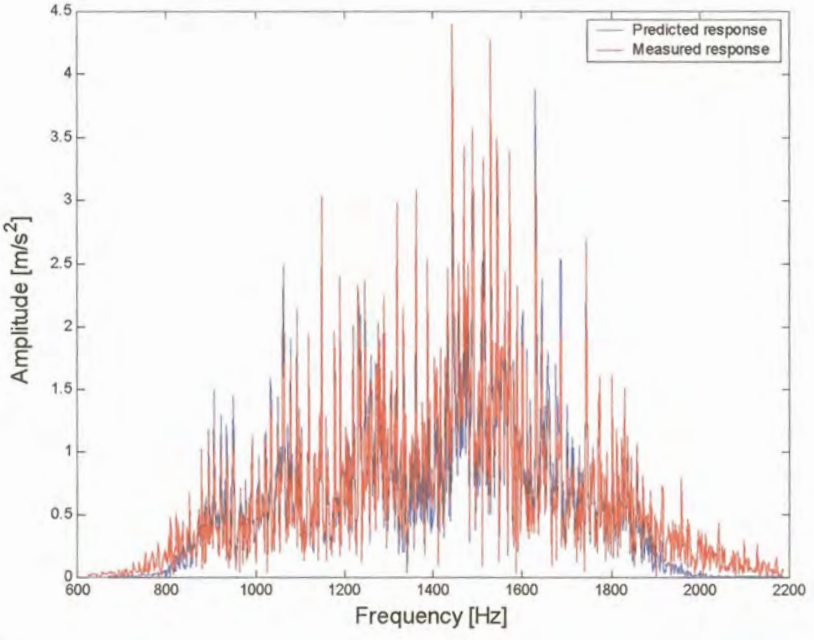

Figure 4.8 (b) *Comparison between the measured and predicted response in the vertical direction*

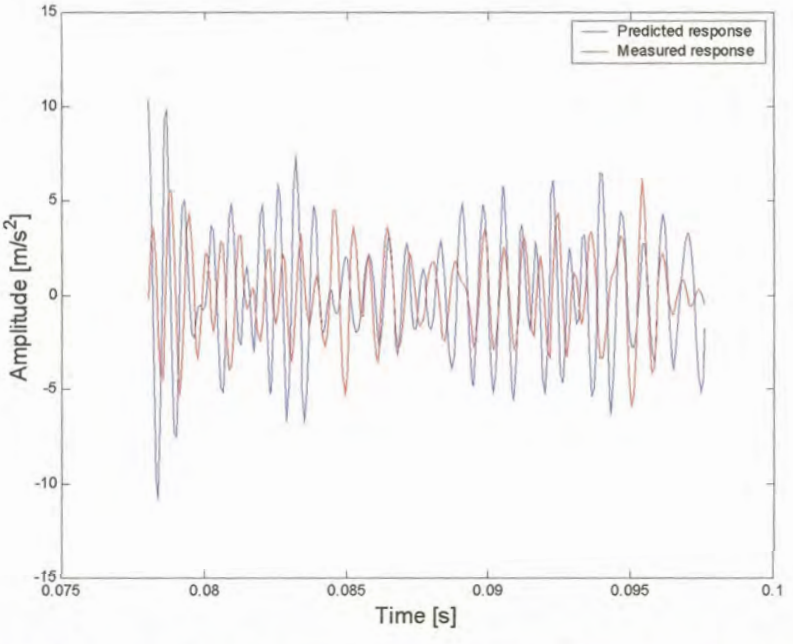

Figure 4.8 (c) *Comparison between the measured and predicted response in the horizontal direction*

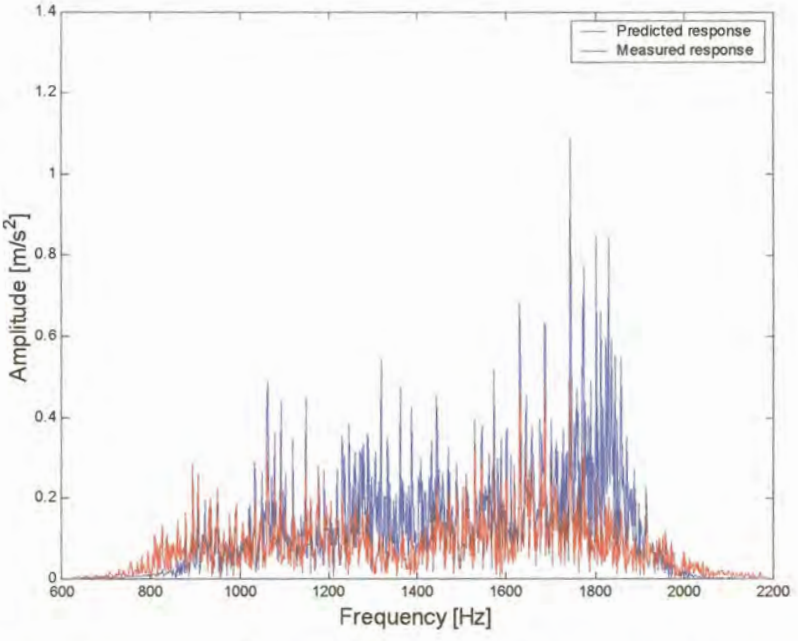

Figure 4.8 (d) *Comparison between the measured and predicted response in the horizontal direction*

The response of the structure in the vertical direction was reconstructed with a correlation of 90.72 percent. Figures 4.8 (a) and (b) indicate the accuracy with which the response was reconstructed. However, the response reconstruction in the horizontal direction was not as successful as the response reconstruction in the vertical direction. The amplitude of the predicted response is larger than the measured response as indicated by the FFT in figure 4.8 (d). The deviation between the two responses can be related to the accuracy with which the model describes the dynamic characteristics of the system. The modal model is merely a linear approximation of the real system. The main objective was to compute input forces that would reconstruct the response of the tool holder in the vertical direction since the research objective was set to attenuate the response in the vertical direction. Therefore the input forces will facilitate an accurate simulation of the cutting process in the vertical direction of the tool holder. The calculated force signals are presented in figures 4.9 a to d.

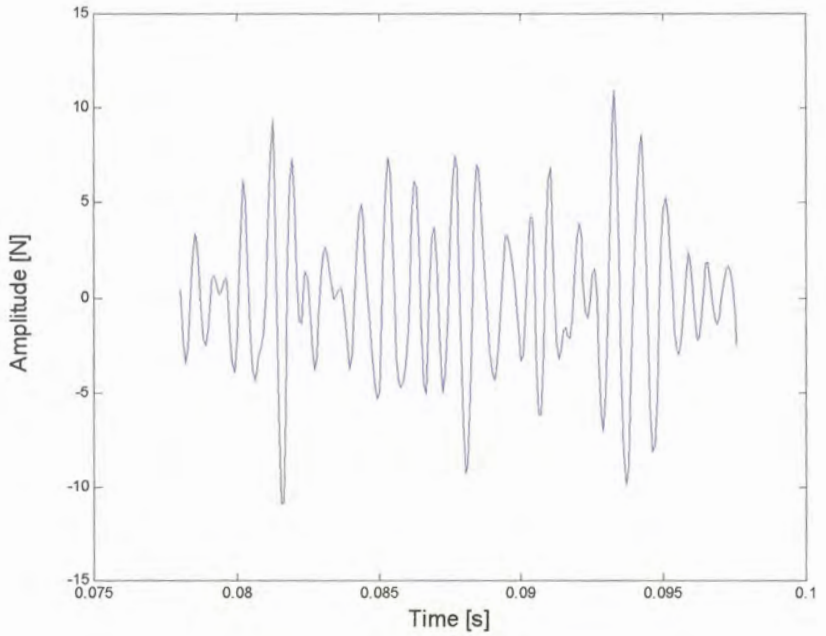

Figure 4.9 (a) *Vertical force signal*

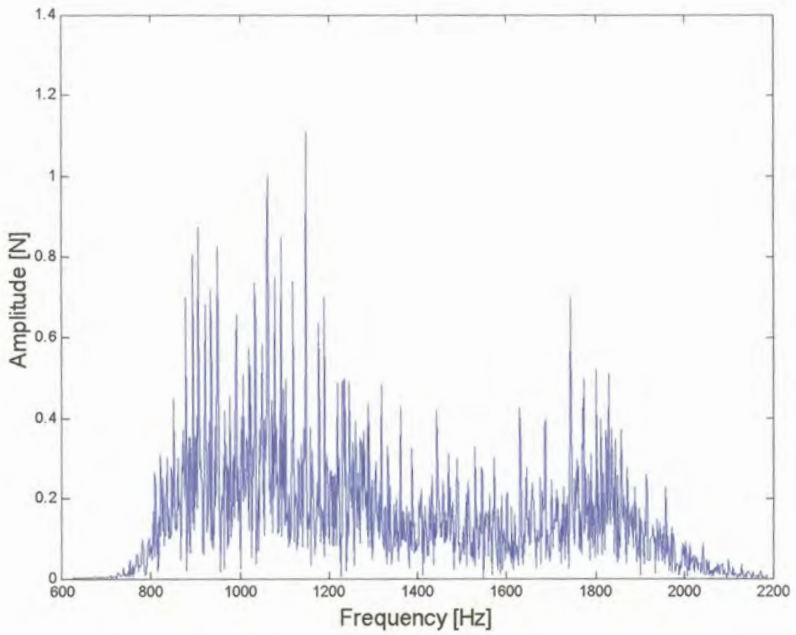

Figure 4.9 (b) *FFT of the vertical force signal*

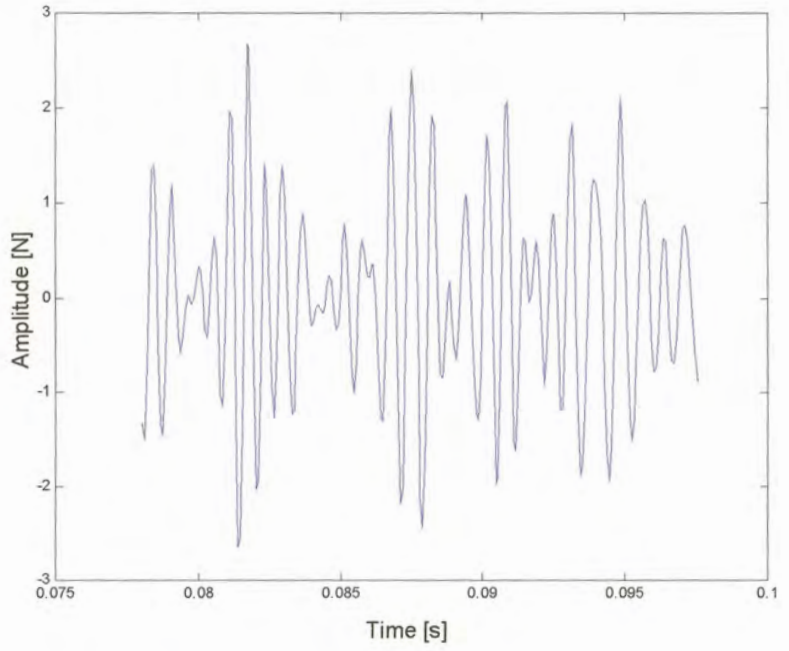

Figure 4.9 (c) *Horizontal force signal*

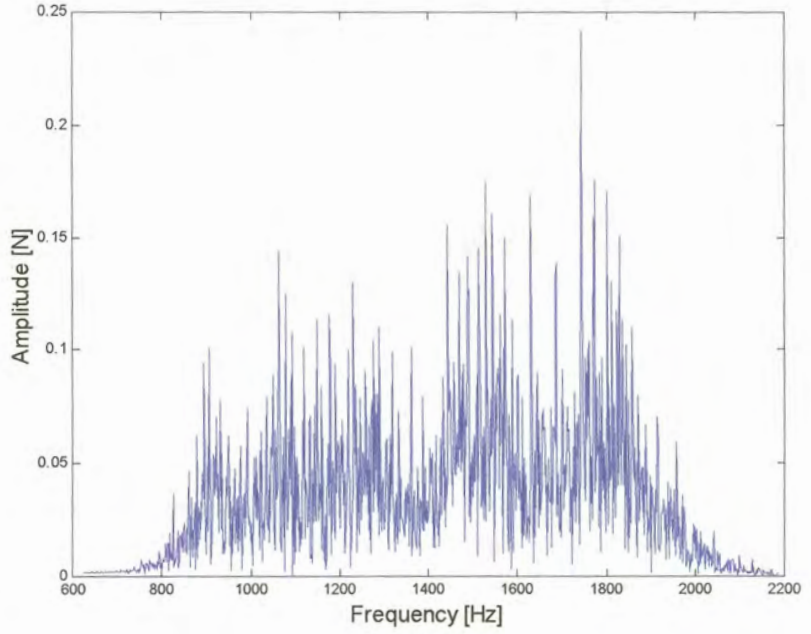

Figure 4.9 (d) *FFT of the horizontal force signal*

Chapter 5

Absorber implementation

The ODS and modal analysis indicated that the most deflection is situated at the tip of the tool in the vertical direction. Therefore the piezoelectric absorber was implemented near the tip of the tool holder in order to manipulate the dynamic stiffness of the cutting edge as much as possible.

A support structure is required to support the actuator in the vertical position. In chapter two the assumption of a rigid support was made since the stiffness of the steel tabletop far exceeded the stiffness of the aluminium beam. However, it is impossible to design a support structure that would fit on the tool changer which would not influence the dynamic characteristics of the system. The influence might improve the dynamic characteristics or it might not. Inevitably an optimal support design is required to ensure optimal performance of the damper in the system. The design of such a support is beyond the scope of the research since the aim is to establish whether the concept is viable.

The support structure is assumed to be rigid in the simulations. Therefore the influence of the support structure is omitted from the modelling process. The influence of the piezoelectric absorber can therefore be determined in isolation. The results obtained from the simulation represents the best scenario, which may be achieved by the implementation of the piezoelectric absorber near the tip of the tool.

5.1 State space modal model of the tool holder and shank

A state space modal model with three force inputs is required to model the structure and the damper. Two of the force inputs are used to simulate the cutting forces of the machining process, as determined in chapter four, while the third input is used in the feedback loop of the piezoelectric damper model. According to Balmés [40] a modal analysis with a collocated transfer function at each force input position is required to construct such a model. Therefore two sets of FRFs were measured with collocated transfer functions at the cutting force input positions, while the third set was measured with a collocated transfer function at the intended actuator position. The modal state space model is an average representation of the modal characteristics of the structure. Figures 5.1 (a) and (b) indicate the transfer function measurements at the collocated point were the actuator would be attached.

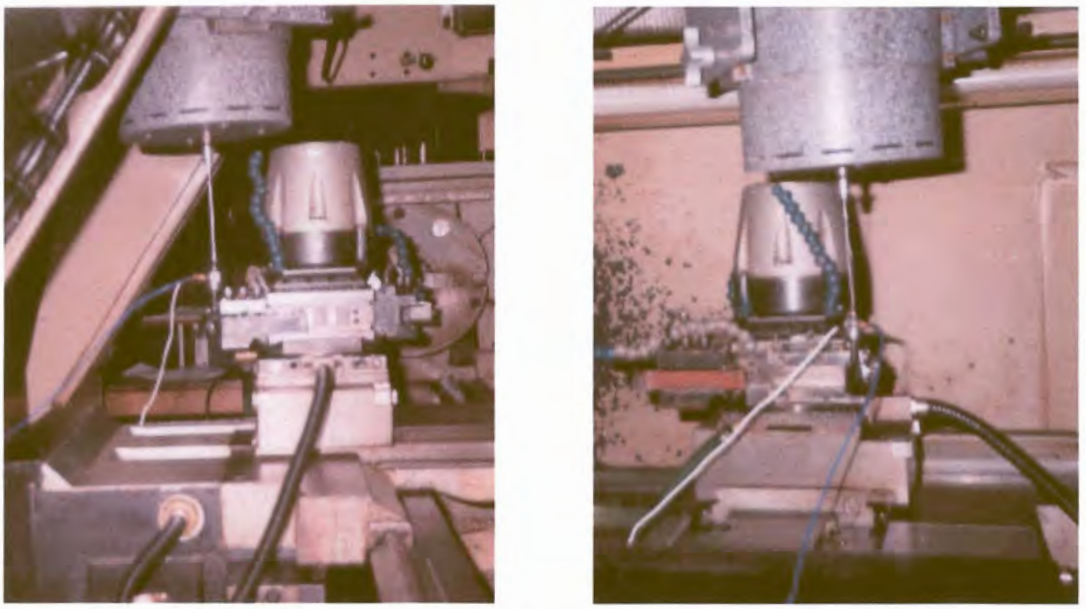

(a) (b)

Figure 5.1 *Transfer function measurement at the actuator attachment position*

5.2 Modelling Process

The objective of the modelling process is to implement and predict the influence of a variety of piezoelectric stack actuators, which are commercially available, as absorbers on the tool holder and shank. The properties of the actuators are substituted in to the feedback loop transfer function of the damper to simulate their behaviour. The optimal resistance and inductance values for the various shunt circuits are determined through inspection. The inspection is based on the transfer function manipulation between the force input and the response at the tool tip in the vertical direction. A schematic representation of the model is shown in figure 5.2.

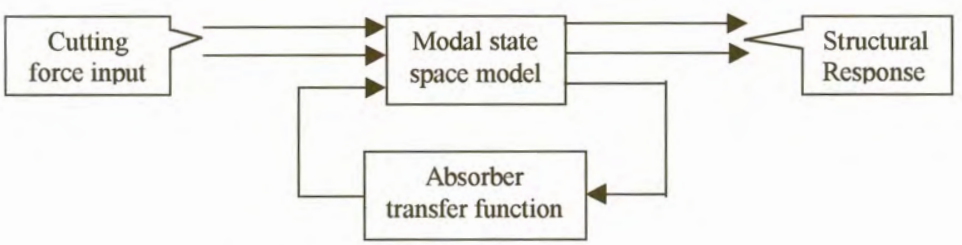

Figure 5.2 *Schematic diagram of the modelling process*

The static stiffness of the actuators is neglected since the open pole static stiffness of the actuators would influence the dynamic characteristics of the tool holder and shank.

To incorporate the open pole static stiffness would be inappropriate since the influence of the support structure is neglected to enable the validation of various dampers on the same structural system. A visual interpretation of the intended configuration is shown in figure 5.3. Note that the static stiffness K of the flow diagram presented in figure 2.1 is neglected in figure 5.3 since the value represents the open pole static stiffness of the actuator.

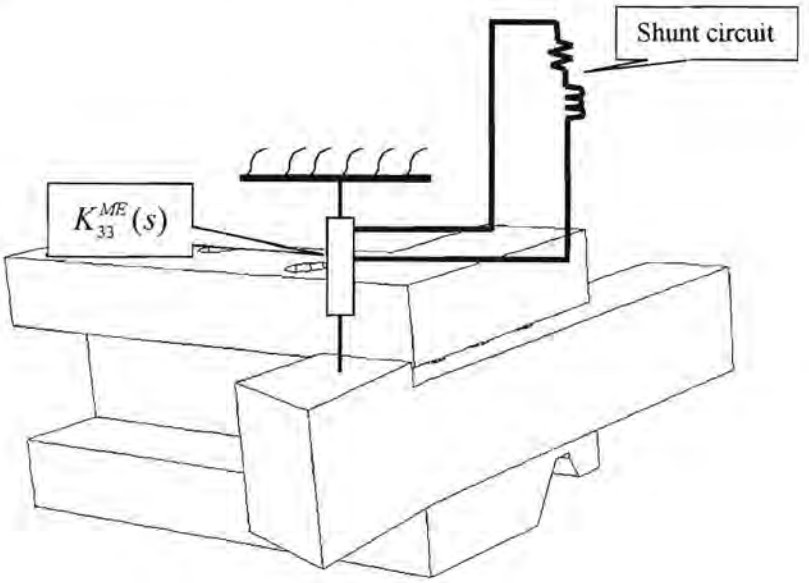

Figure 5.3 *Visual representation of the piezoelectric damper implementation on the tool holder and shank*

A selection of six actuators from Piezomechanik was simulated. The specifications of the actuators are tabled in table 5.1 (a) and (b).

Table 5.1 (a) Piezomechnik piezoelectric stack actuators

Actuator model	Diameter [m]	Number of layers	Layer thickness [m]	Capacitance [F]
500/5/5	0.005	14	3.5×10^{-4}	40×10^{-9}
500/5/15	0.005	42	3.5×10^{-4}	100×10^{-9}
500/5/25	0.005	72	3.5×10^{-4}	150×10^{-9}
500/10/5	0.01	14	3.5×10^{-4}	150×10^{-9}
500/10/15	0.01	42	3.5×10^{-4}	400×10^{-9}
500/10/25	0.01	72	3.5×10^{-4}	600×10^{-9}

Table 5.1 (b) Material properties of the Piezomechnik piezoelectric stack actuators

Relative dielectric constant	4000
Piezoelectric charge constant	500×10^{-12} [m/V]
Young's modulus	60×10^{9} [N/m^2]

5.3 FRF simulation results

The FRF simulation entailed the attenuation of three structural modes with the various piezoelectric absorbers formed with the actuator properties indicated in section 5.2. The three structural mode frequencies and damping levels are presented in table 5.2.

Table 5.2 Structural modes attenuated in the simulations

Mode frequency [Hz]	Damping [%]
1847.2	3.99
1639.9	10.91
1098.7	5.28

The frequency response of the 1639.9 Hz mode is increased when the absorber is tuned to the 1582.2 Hz mode. This can be related to the fact that the mode formed by the absorber is near the mode of the structure at 1639.9 Hz. However if the absorber is tuned to the mode at 1639.9 Hz, it attenuates the FRF at the 1582.2 Hz mode. Therefore the 1639.9 Hz mode was selected for the investigation. The amount of attenuation was measured between the original FRF value at 1582.2 Hz and the peak FRF value at the absorbed mode frequency. The amounts of attenuation for the other two structural modes are measured between the original FRF value of the mode and value of the mode when absorbed.

The results of the simulation are presented in tables 5.3 (a) to (c) and 5.4 (a) to (c). The FRFs for the simulations are displayed in figures 5.4 (a) to (c) and 5.5 (a) to (c).

Table 5.3 (a) Attenuation results at the 1847.2 Hz mode with the 500/5/- series piezoelectric actuators

Actuator	Resistance [Ω]	Inductance [H]	Attenuation [ms^2/N]	Attenuation [%]
500/5/5	80	0.197	2.95	11.68
500/5/15	40	0.099	3.9	15.44
500/5/25	35	0.0764	2.79	11.04

Table 5.3 (b) Attenuation results at the 1639.9 Hz mode with the 500/5/- series piezoelectric actuators

Actuator	Resistance [Ω]	Inductance [H]	Attenuation [ms^2/N]	Attenuation [%]
500/5/5	400	0.234	1.99	9.25
500/5/15	350	0.130	2.56	11.89
500/5/25	220	0.11	2.25	10.40

Table 5.3 (c) Attenuation results at the 1098.7 Hz mode with the 500/5/- series piezoelectric actuators

Actuator	Resistance [Ω]	Inductance [H]	Attenuation [ms^2/N]	Attenuation [%]
500/5/5	350	0.68	2.62	27.5
500/5/15	150	0.345	1.57	16.526
500/5/25	90	0.254	1.04	10.80

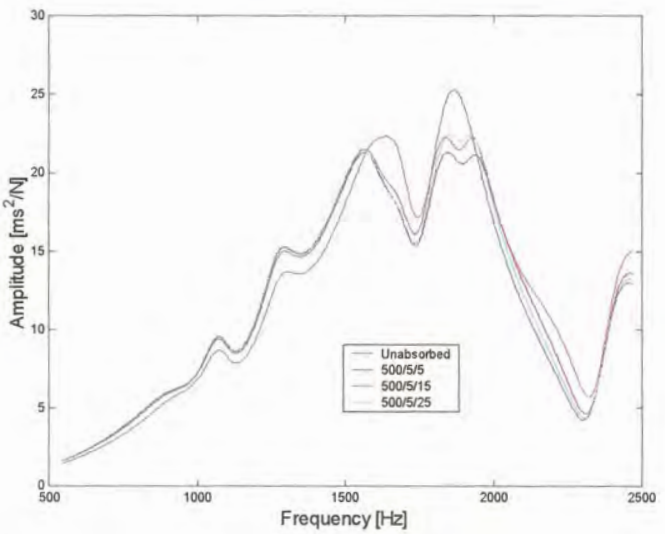

Figure 5.4 (a) *FRFs of the attenuation results at the 1847,2 Hz mode with the 500/5/- series piezoelectric actuators*

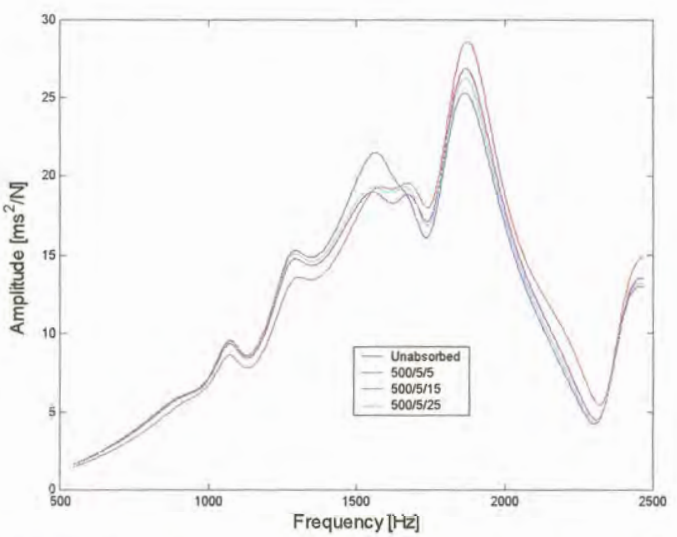

Figure 5.4 (b) *FRFs of the attenuation results at the 1639,9 Hz mode with the 500/5/- series piezoelectric actuators*

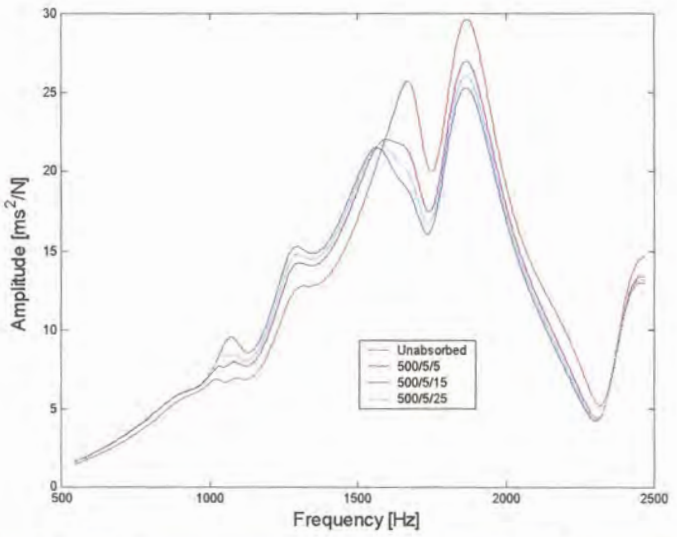

Figure 5.4 (c) *FRFs of the attenuation results at the 1098,7 Hz mode with the 500/5/- series piezoelectric actuators*

Table 5.4 (a) Attenuation results at the 1847.2 Hz mode with the 500/10/- series piezoelectric actuators

Actuator	Resistance [Ω]	Inductance [H]	Attenuation [ms²/N]	Attenuation [%]
500/10/5	19	0.049	Unavailable	Unavailable
500/10/15	10	0.022	4.42	17.5
500/10/25	8	0.017	4.61	18.23

Table 5.4 (b) Attenuation results at the 1639.9 Hz mode with the 500/10/- series piezoelectric actuators

Actuator	Resistance [Ω]	Inductance [H]	Attenuation [ms²/N]	Attenuation [%]
500/10/5	45	0.061	0.94	4.37
500/10/15	60	0.024	2.25	26.84
500/10/25	90	0.021	2.46	11.43

Table 5.4 (c) Attenuation results at the 1098.7 Hz mode with the 500/10/- series piezoelectric actuators

Actuator	Resistance [Ω]	Inductance [H]	Attenuation [ms²/N]	Attenuation [%]
500/10/5	60	0.163	2.45	25.79
500/10/15	40	0.077	2.55	26.84
500/10/25	30	0.059	1.98	20.8

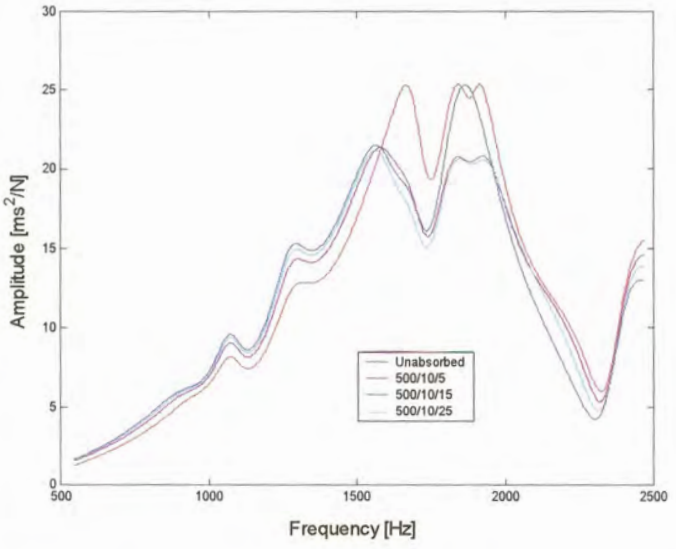

Figure 5.5 (a) *FRFs of the attenuation results at the 1847.2 Hz mode with the 500/10/- series piezoelectric actuators*

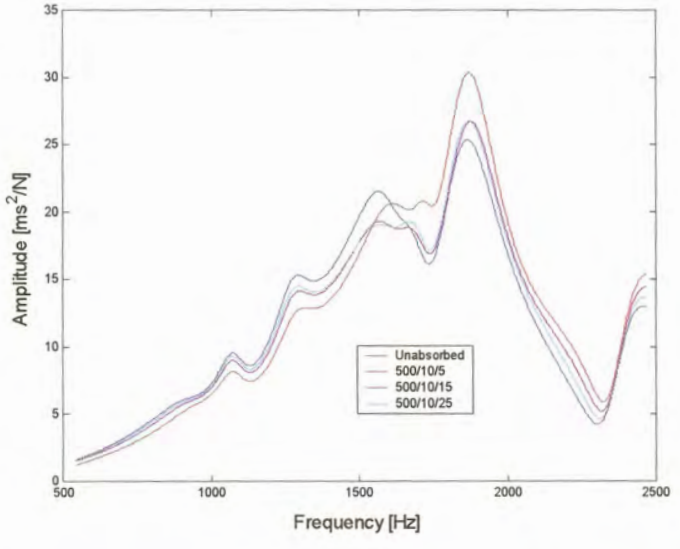

Figure 5.5 (b) *FRFs of the attenuation results at the 1639.9 Hz mode with the 500/10/- series piezoelectric actuators*

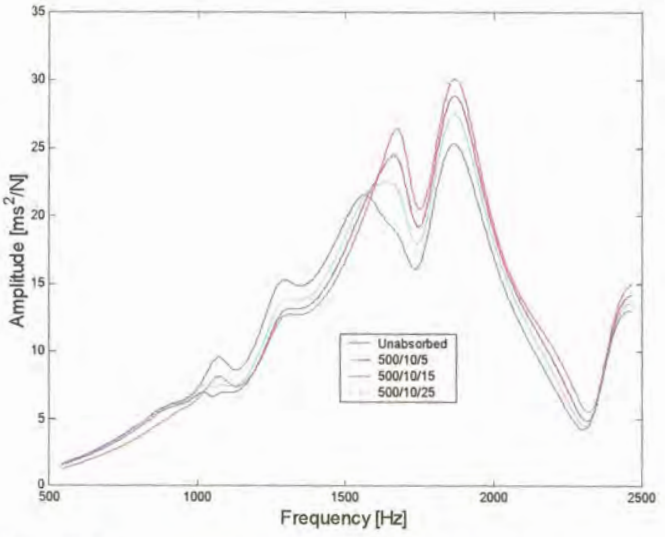

Figure 5.5 (c) *FRFs of the attenuation results at the 1098.7 Hz mode with the 500/10/- series piezoelectric actuators*

The shunt circuit of the piezoelectric absorber is tuned to a specific resonant frequency to absorb a structural mode. However, the resonant frequency of the shunt circuit is a function of the capacitance, inductance and resistance values of the circuit. Therefore, the resistance and inductance values are decreased when the capacitance value of the actuator is increased.

The absorber simulations with the 500/10/- series of actuators on the 1639.9 Hz mode indicated an increase in the resistance values as the capacitance value was increased. Therefore, the previous assumption is invalid when the absorber is influenced by structural modes with frequency values near the mode that is being absorbed.

The amount of damping in the absorber should be more than the amount of inherent damping present in the structural mode, in order to attenuate the structural mode. Resistance is the equivalent of damping in an electrical circuit, and therefore the resistance value of the shunt circuit is related to the inherent damping level present in the absorbed structural mode. The results of the simulations indicate a rise in the resistance values as the inherent mode damping increases.

The resistance values for the various actuator simulations on the three structural modes are shown in tables 5.5 (a) and (b).

Table 5.5 (a) Optimal resistance values for the various modes and actuators of the 500/5/- range

Actuator	Mode 1098.7 Hz Damping 3.99 % Resistance [Ω]	Mode 1639.9 Hz Damping 10.91 % Resistance [Ω]	Mode 1847.2 Hz Damping 5.28 % Resistance [Ω]
500/5/5	80	400	350
500/5/15	40	350	150
500/5/25	35	220	90

Table 5.5 (b) Optimal resistance values for the various modes and actuators of the 500/10/- range

Actuator	Mode 1098.7 Hz Damping 3.99 % Resistance [Ω]	Mode 1639.9 Hz Damping 10.91 % Resistance [Ω]	Mode 1847.2 Hz Damping 5.28 % Resistance [Ω]
500/10/5	19	45	60
500/10/15	10	60	40
500/10/25	8	90	30

Unfortunately, the addition of the piezoelectric absorber may cause an increase in the FRF values at other frequencies of the system. The extent of the phenomena seems to be related to the aspect ratio of the actuator. The definition of the actuator aspect ratio is presented in equation 5.1.

$$\text{Aspect ratio} = \frac{\text{Actuator diameter}}{\text{Actuator length}} \tag{5.1}$$

The increase in the FRF values is tabled in tables 5.6 (a) to (f), along with the aspect ratio of the actuators for the various simulations.

Table 5.6 (a) Increase in the FRF value at 1639.9 Hz, due to the attenuation of the mode at 1847.2 Hz with the 500/5/- series of actuators

Actuator	Capacitance [H]	Aspect ratio	Increase in the FRF value [ms^2/N]
500/5/5	40×10^{-9}	1	0.87
500/5/15	100×10^{-9}	0.33...	No increase
500/5/25	150×10^{-9}	0.2	No increase

Table 5.6 (b) Increase in the FRF value at 1847.2 Hz, due to the attenuation of the mode at 1639.9 Hz with the 500/5/- series of actuators

Actuator	Capacitance [H]	Aspect ratio	Increase in the FRF value [ms^2/N]
500/5/5	40×10^{-9}	1	3.36
500/5/15	100×10^{-9}	0.33...	1.57
500/5/25	150×10^{-9}	0.2	0.97

Table 5.6 (c) Increase in the FRF value at 1847.2 Hz, due to the attenuation of the mode at 1098.7 Hz with the 500/5/- series of actuators

Actuator	Capacitance [H]	Aspect ratio	Increase in the FRF value [ms^2/N]
500/5/5	40×10^{-9}	1	4.37
500/5/15	100×10^{-9}	0.33...	1.70
500/5/25	150×10^{-9}	0.2	0.79

Table 5.6 (d) Increase in the FRF value at 1639.9 Hz, due to the attenuation of the mode at 1847.2 Hz with the 500/10/- series of actuators

Actuator	Capacitance [H]	Aspect ratio	Increase in the FRF value [ms^2/N]
500/10/5	150×10^{-9}	2	3.78
500/10/15	400×10^{-9}	0.66...	No increase
500/10/25	600×10^{-9}	0.4	No increase

Table 5.6 (e) Increase in the FRF value at 1847.2 Hz, due to the attenuation of the mode at 1639.9 Hz with the 500/10/- series of actuators

Actuator	Capacitance [H]	Aspect ratio	Increase in the FRF value [ms^2/N]
500/10/5	150×10^{-9}	2	5.12
500/10/15	400×10^{-9}	0.66...	1.43
500/10/25	600×10^{-9}	0.4	1.46

Table 5.6 (f) Increase in the FRF value at 1847.2 Hz, due to the attenuation of the mode at 1098.7 Hz with the 500/10/- series of actuators

Actuator	Capacitance [H]	Aspect ratio	Increase in the FRF value [ms^2/N]
500/10/5	150×10^{-9}	2	4.79
500/10/15	400×10^{-9}	0.66...	3.57
500/10/25	600×10^{-9}	0.4	2.19

The increase in the FRF values, due to the absorber implementation, decreases as the aspect ratio of the actuator decreases. The 500/10/5 and the 500/5/25 actuators both have a capacitance value of 150×10^{-9} F but has aspect ratios of 2 and 0.2 respectively. Tables 5.6 (c) and (d) indicates that the 500/10/5-actuator ads a minimum of 3.78 ms^2/N to the FRF while the 500/5/25 ads a maximum of 0.97 ms^2/N. Therefore the FRF value increase is primarily related to the aspect ratio of the actuator and not the capacitance value of the actuator.

The attenuation versus capacitance results is presented in table 5.7 (a) and (b). The amount of attenuation increases and decreases when the capacitance value is increased. Therefore the assumption made in section 2.4.2 regarding the increase in attenuation with the increase in capacitance is incorrect for multiple degree of freedom systems.

Table 5.7 (a) Percentage attenuation for each mode versus the capacitance values of the 500/5/- actuator series

Actuator	Capacitance [H]	Aspect ratio	Attenuate of the mode at 1847.2 Hz [%]	Attenuate of the mode at 1639.9 Hz [%]	Attenuate of the mode at 1098.7 Hz [%]
500/5/5	40×10^{-9}	1	11.68	9.25	27.50
500/5/15	100×10^{-9}	0.33...	15.44	11.89	16.526
500/5/25	150×10^{-9}	0.2	11.04	10.4	10.8

Table 5.7 (b) Percentage attenuation for each mode versus the capacitance values of the 500/10/- actuator series

Actuator	Capacitance [H]	Aspect ratio	Attenuate of the mode at 1847.2 Hz [%]	Attenuate of the mode at 1639.9 Hz [%]	Attenuate of the mode at 1098.7 Hz [%]
500/10/5	150×10^{-9}	2	Unavailable	4.37	25.79
500/10/15	400×10^{-9}	0.66...	17.50	10.46	26.84
500/10/25	600×10^{-9}	0.4	18.23	11.43	20.80

The average attenuation results vary between ten and twenty percent and the amount of attenuation obtained by the implementation of the absorber is a function of the dynamic properties of the structure, the capacitance and aspect ratio of the actuator. A graphical representation of the results in tables 5.7 (a) and (b) is presented in figures 5.6 (a) and (b).

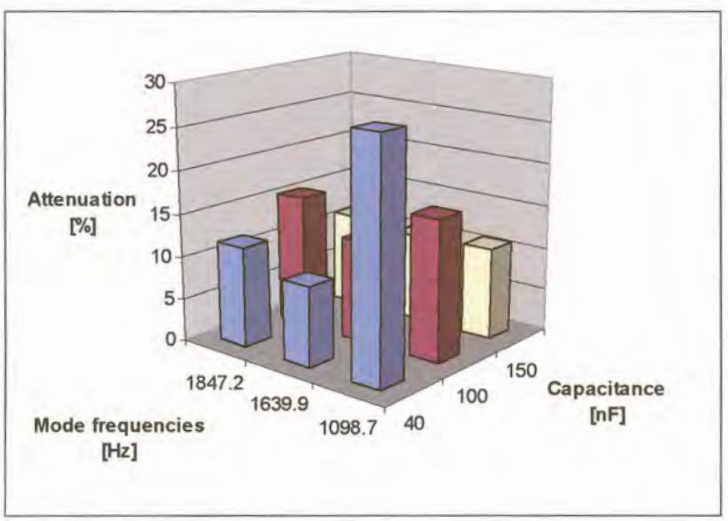

Figure 5.6 (a) *Attenuation results versus the capacitance values for the simulations with the 500/5/- series of actuators*

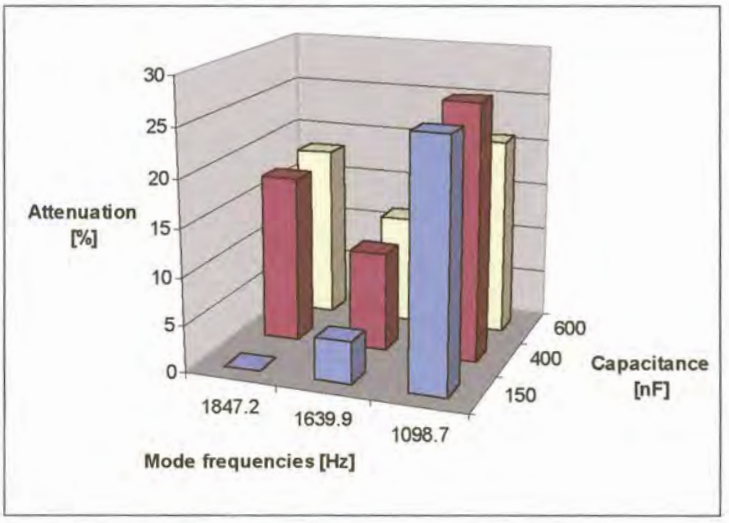

Figure 5.6 (b) *Attenuation results versus the capacitance values for the simulations with the 500/10/- series of actuators*

5.4 Cutting process simulation

The 500/5/15 piezoelectric actuator exhibits superior attenuation ability and minimal disturbance of the FRF over the remainder of the frequency bandwidth. Therefore the actuator was implemented in the cutting process simulation. The results of the simulations are presented in table 5.8 and figures 5.7 (a) to (f).

Table 5.8 Cutting process simulation results

Absorbed mode	FRF attenuation [%]	Amplitude attenuation of the time response signal [$\%_{RMS}$]
1847.2 Hz	15.44	2.93
1639.9 Hz	11.89	3.49
1098.7 Hz	16.53	5.51

Equation 5.2 expresses the amount of attenuation obtained in the cutting process simulation.

$$\text{Atenuation} = \frac{\text{Unabsorbed response amplitude}_{RMS} - \text{Absorbed response amplitude}_{RMS}}{\text{Unabsorbed response amplitude}_{RMS}} \times 100 \quad (5.2)$$

A small amount of attenuation is obtained in the cutting process since the structure is exposed to a wide band excitation of 1200 Hz during the cutting process and the absorber only attenuates an effective frequency bandwidth of approximately 50 to 100 Hz.

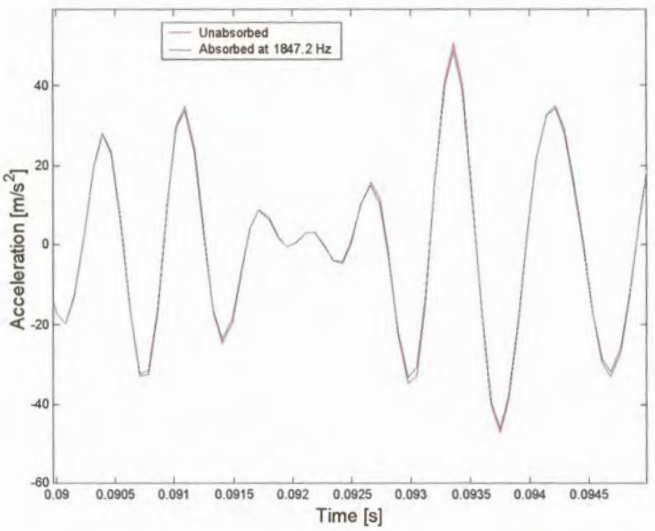

Figure 5.7 (a) *Response in the vertical direction at the tool tip during the cutting simulation with the 1847.2 Hz mode attenuated*

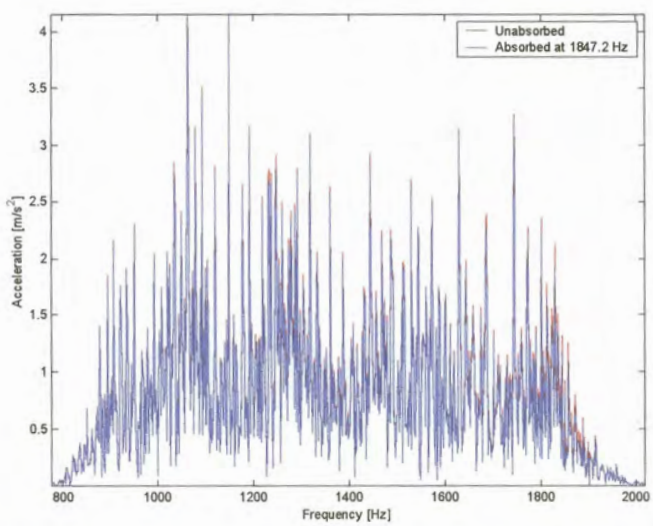

Figure 5.7 (b) *FFT of the response in the vertical direction at the tool tip during the cutting simulation with the 1847.2 Hz mode attenuated*

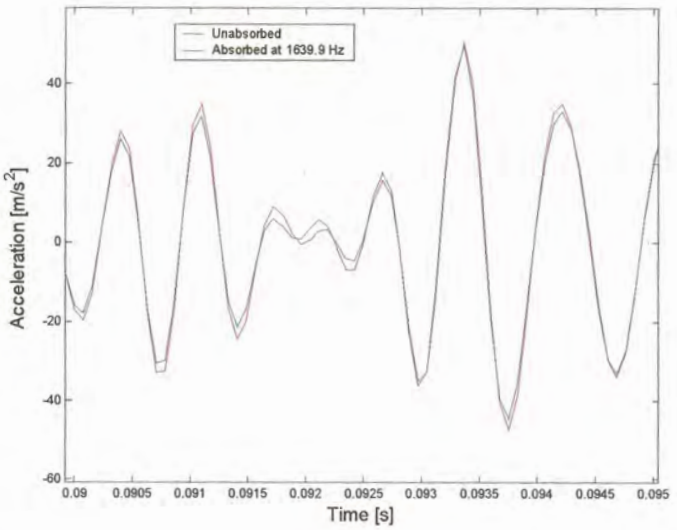

Figure 5.7 (c) *Response in the vertical direction at the tool tip during the cutting simulation with the 1639.9 Hz mode attenuated*

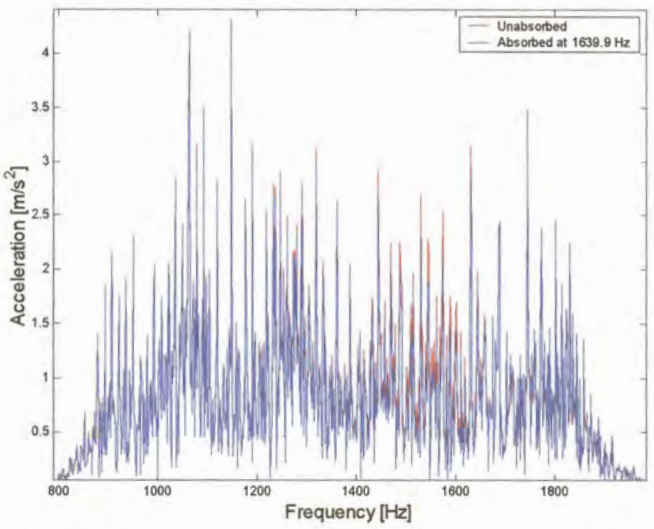

Figure 5.7 (d) *FFT of the response in the vertical direction at the tool tip during the cutting simulation with the 1639.9 Hz mode attenuated*

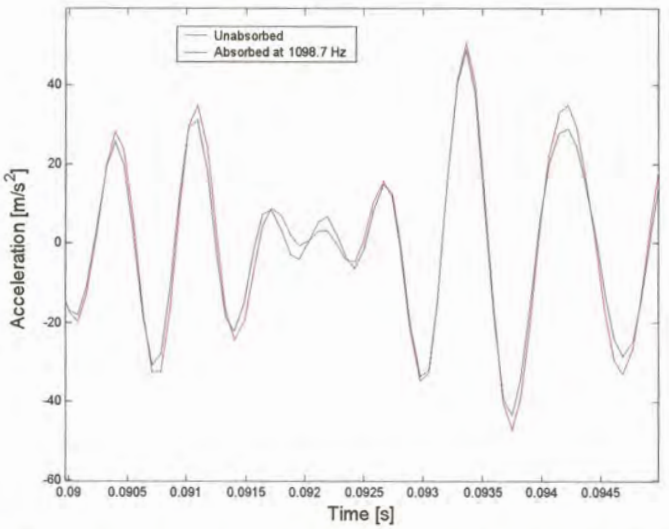

Figure 5.7 (e) *Response in the vertical direction at the tool tip during the cutting simulation with the 1098.7 Hz mode attenuated*

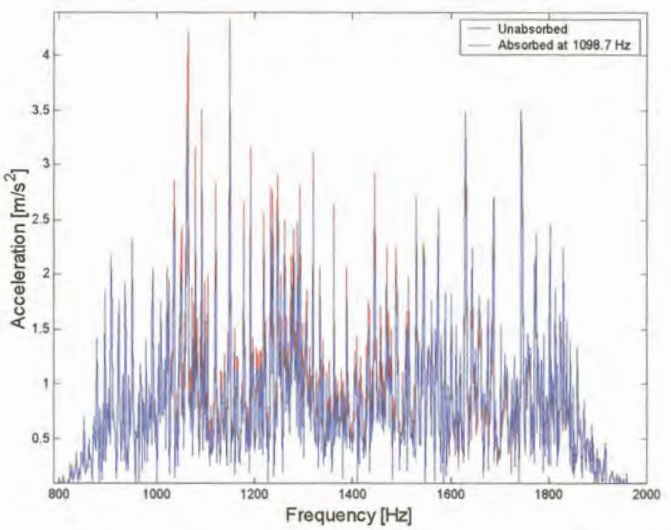

Figure 5.7 (f) *FFT of the response in the vertical direction at the tool tip during the cutting simulation with the 1098.7 Hz mode attenuated*

5.5 Cutting process simulation with multiple absorbers

The objective of the multiple absorber implementation is to increase the effective bandwidth of attenuation. Three absorbers were implemented at the absorber connection point to attenuate the three modes simultaneously, in a bid to improve the attenuation results. Slight changes to the shunt circuit inductance values had to be made since the absorbers influenced one another.

The FRF result of the multiple absorber implementation is displayed in figure 5.8 (a). The amount of attenuation obtained by the absorber implementation at the 1847.2 Hz mode decreased considerably. However the bandwidth of effective attenuation was increased between the 1098.7 Hz and 1639.9 Hz modes.

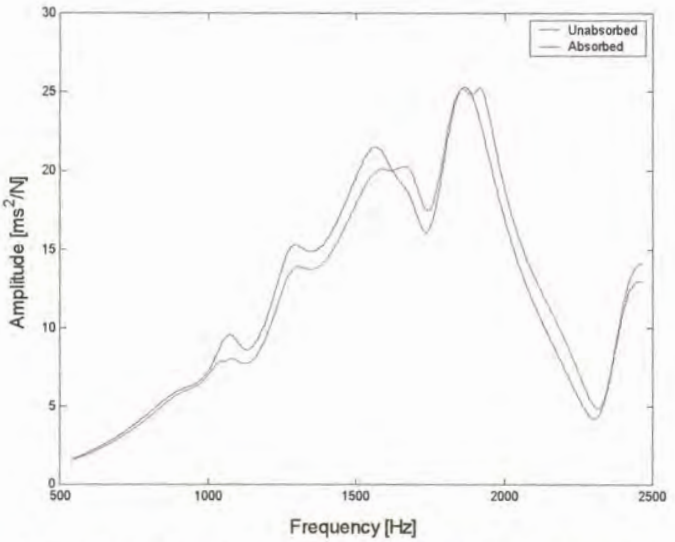

Figure 5.8 (a) *FRF result of the multiple absorber implementation*

The multiple absorber implementation increased the amount of attenuation during the cutting process to 8.76 $\%_{RMS}$. Figures 5.8 (b) and (c) reveal the results obtained by the cutting process.

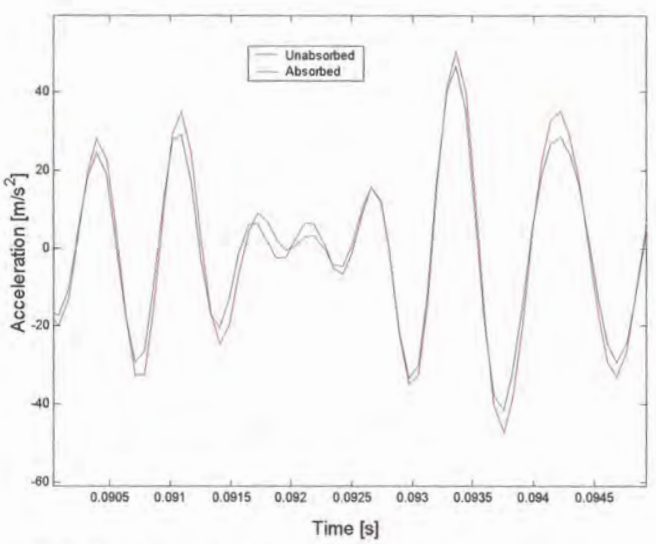

Figure 5.8 (b) *Result of the multiple absorber implementation*

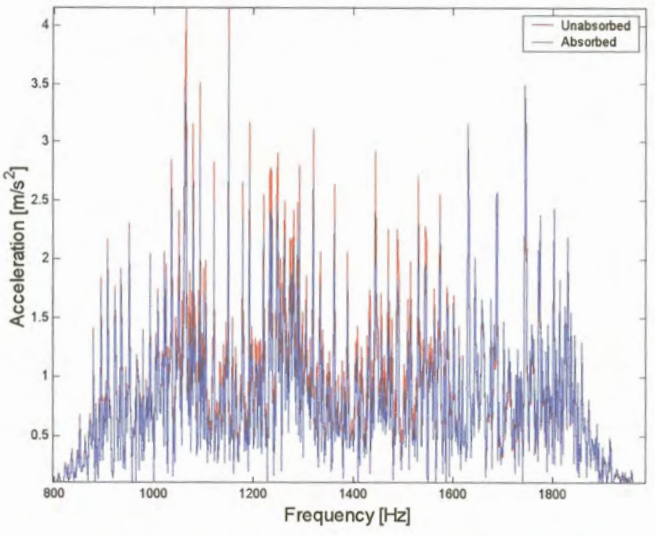

Figure 5.8 (c) R*esult of the multiple absorber implementation*

The attenuation results did not improve as much as expected due to the influence the dampers have on one another.

5.6 Experimental verification

The assembly of the structural support and the piezoelectric stack actuator is presented in figures 5.9 (a) and (b).

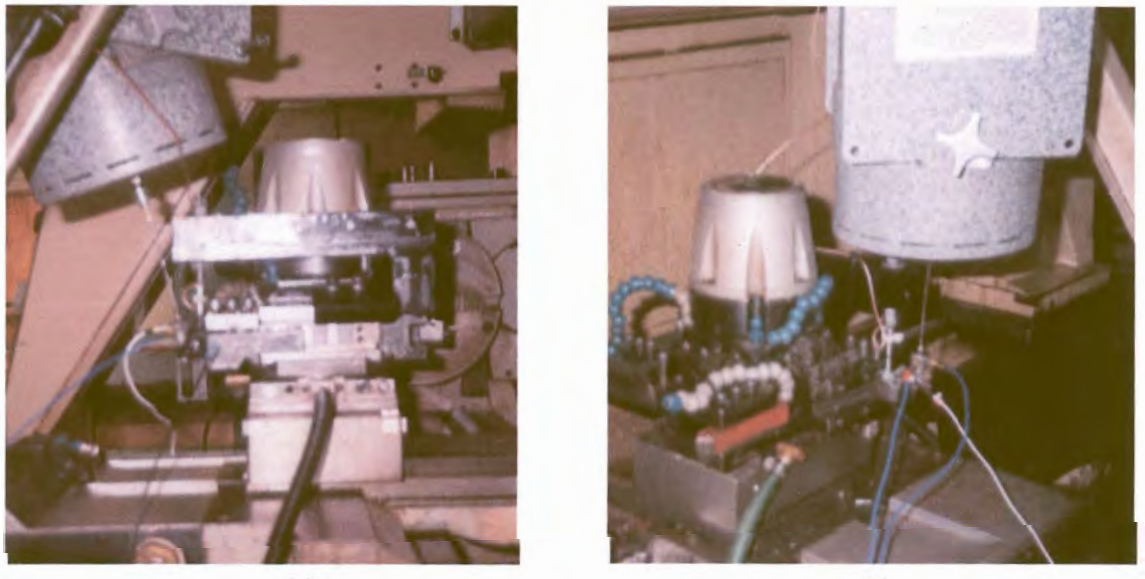

(a) (b)

Figure 5.9 *Piezoelectric absorber implementation on the tool holder for the experimental verification*

A 500/5/15 piezoelectric stack actuator from piezomechanik was implemented in the experimental verification of the piezoelectric absorber on the lathe. The addition of the structural support and piezoelectric stack actuator influenced the dynamic characteristics of the system. A modal analysis was conducted to determine the new modal properties of the system as indicated in figures 5.10 (a) to (e). The mode frequencies of the new system are tabled in table 5.9.

Table 5.9 Mode properties of the system with the structural support in the vertical direction

Mode frequency [Hz]	Damping value [%]
813.2	5.71
1274.6	4.38
1531.5	2.68
1735.8	8.22
1878.8	3.62
1930.8	2.73

The piezoelectric absorber was tuned to absorb the 813.2 Hz, 1735.8 Hz and 1930.8 Hz modes during the experimental verification. Figures 5.10 (a) to (e) displays the point inertance at the tip of the tool holder that were measured to determine the influence of the absorber. The results of the experimental verification are tabled in table 5.10.

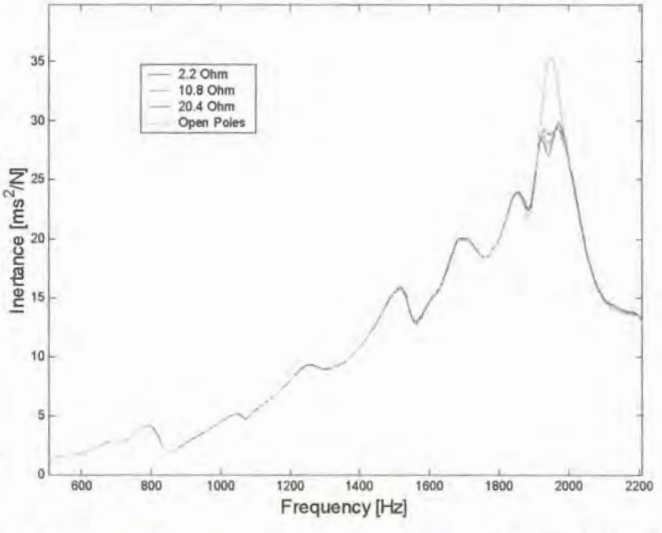

Figure 5.10 (a) Experimental absorption results at the 1930.8 Hz mode

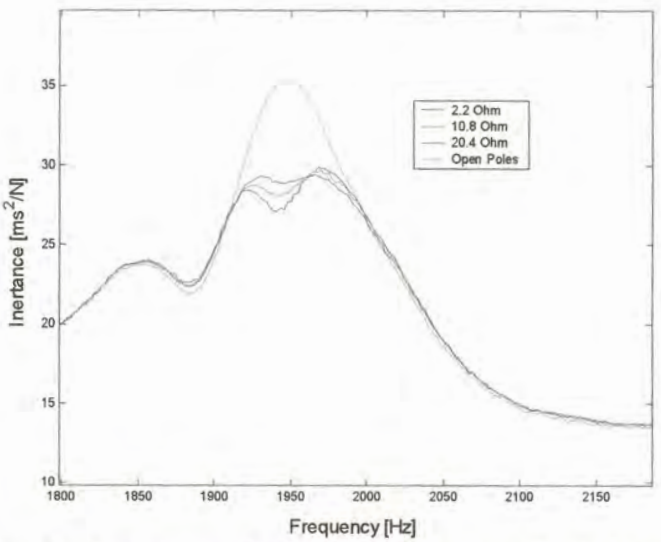

Figure 5.10 (b) Experimental absorption results at the 1930.8 Hz mode

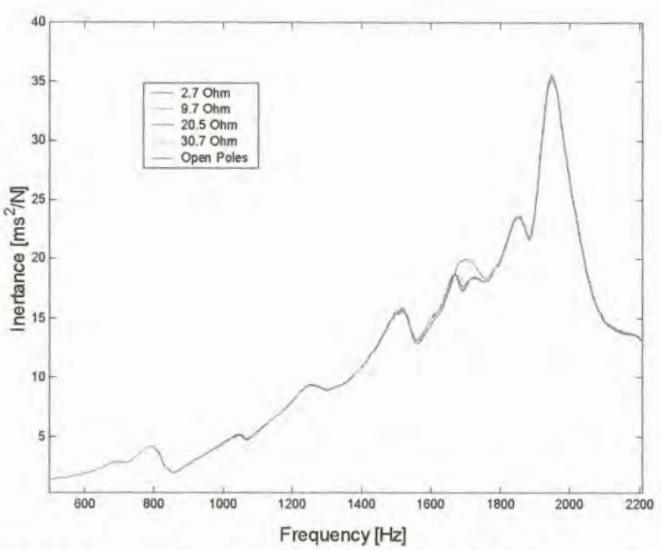

Figure 5.10 (c) Experimental absorption results at the 1735.8 Hz mode

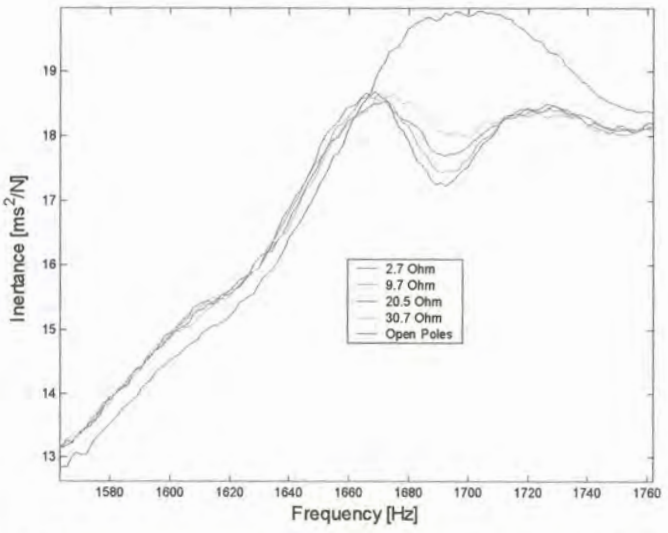

Figure 5.10 (d) Experimental absorption results at the 1735.8 Hz mode

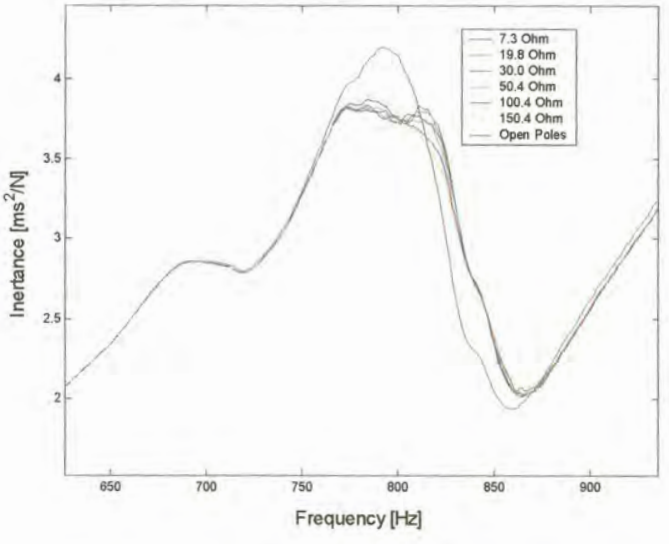

Figure 5.10 (e) Experimental absorption results at the 813.2 Hz mode

Table 5.10 Results of the experimental verification

Mode frequency[Hz]	Resistance [Ω]	Inductance [H]	Attenuation [ms²/N]	Attenuation [%]
813.2	7.3	0.8734	0.37	8.77
1735.8	20.5	0.2221	1.41	7.05
1930.8	20.4	0.1673	6.12	17.23

The experimental implementation of the absorber on the tool holder was successful and the magnitudes of the attenuation results were within the regions predicted by the mathematical simulations. However, the average inductance values required in the shunt circuit of the absorber were higher than the values required in the mathematical simulation since the real capacitance value of the actuator is approximately 74×10^{-9} F. Therefore higher inductance values were required to compensate for the loss in capacitance in order to obtain the correct resonance frequency for the piezoelectric absorber.

Minimal disturbance of the FRF bandwidth was noted in the experimental verification results due to the addition of the support structure and static stiffness of the actuator which influenced the system.

Table 5.11 indicates the optimal shunt resistance versus the damping value of the three structural modes. The experimental results do not verify the conclusion made in section 5.4 about the relationship between the required resistance and the level of inherent damping of the structural mode that is absorbed. The occurrence can also be related to the addition of the support structure and static stiffness of the actuator.

Table 5.11 Mode damping versus the shunt resistance results

Mode frequency[Hz]	Resistance [Ω]	Damping value [%]
813.2	7.3	5.71
1735.8	20.5	8.22
1930.8	20.4	2.73

Unfortunately the influence of the piezoelectric absorber could not be verified experimentally during the cutting process since no measurements could be made with 5 percent repeatability.

Chapter 6

Conclusion and recommendations for future research

6.1 Conclusion

6.1.1 Analysis procedure

An analysis procedure was developed to investigate the implementation of a shunted piezoelectric actuator that will attenuate the vibrations experienced by a machine tool structure during a machining operation.

The behaviour of the machine tool structure under machining conditions was determined with an ODS analysis which assisted the decision of actuator positioning on the structure. The repeatability of the transmissibility measurements taken for the ODS analysis was superior to normal acceleration measurements on the structure since they are less susceptible to the variation in the excitation force of the cutting process.

A modal analysis was conducted on the structure to determine the dynamic properties of the system and to construct a modal state space model, which is used in the simulation processes. The mode shapes of the modal analysis were used to verify the observations made in the ODS analysis.

A transfer function of the shunted piezoelectric actuator was used in a feedback loop to the modal state space model to simulate the influence of the passively shunted piezoelectric actuator on the structure. The mathematical simulation was based on the assumption that the support structure is rigid. The assumption isolates the system from the influences of the support structure and therefore the influence of the shunted piezoelectric actuators could be determined on a structure with the same dynamic properties.

The original FRF was compared to the compensated FRF at the tool tip to select the optimal actuator and to determine the optimal shunt circuit. The machine tool structure is subjected to wide band excitation during the machining process and therefore the system has to be simulated under machining conditions to determine the effectiveness of the shunted piezoelectric device. The input forces to the simulation process were determined through the SDRR technique proposed by Raath [43].

6.1.2 Mathematical model of the shunted piezoelectric actuator

A mathematical model for a shunted piezoelectric stack actuator was derived and verified experimentally on an aluminium-cantilevered beam. Acceptable correlation was obtained between the mathematical and experimental results. However the addition of the actuator to a structure alters the dynamic properties of the system which makes it difficult to predict the behaviour of the system prior to experimental verification.

The manufacturer's specification on the actuator's rated capacitance value is unfortunately not as accurate as required, and the value has to be obtained experimentally.

The mathematical model of the shunted piezoelectric actuator was developed into a transfer function format in order to incorporate the model with a state space model representation of several different structures. Therefore, no mathematical formulas were derived to estimate the required shunt circuit values, since they are dependent on the structural properties.

6.1.3 FEM of the machine tool structure

A FEM of the structure has to be updated by experimental modal analysis, in order to ensure its integrity. It is necessary to match all of the mode frequencies and shapes for the frequency bandwidth of concern. In some of the published research on machine tool structures, merely a few of the mode frequencies are matched, which is insufficient proof of the FEM's integrity and accuracy. However the reason for the attempts are obvious, since it is extremely difficult to update the multiple modes of the model.

Several attempts were made to model the tool holder and shank of the diplomatic tool changer. Unfortunately, none of the attempts succeeded in passing the MAC test. The failure is caused by the inability to model the interaction between the various connections of the model. The modal model is used in the mathematical simulations due to the inaccuracies of the FEM.

6.1.4 Results of the implementation of the shunted piezoelectric stack actuator the tool holder

A piezoelectric absorber was implemented on the tool holder to attenuate the vibration at the tool tip, since it was more effective than the resistive shunt. The implementation was successful and 17 percent attenuation was obtained at one of the modes during the experimental verification. Attenuation levels of up to 27 percent were obtained with the mathematical simulations.

Due to the wide band excitation, the amount of attenuation obtained during the machining process is reduced to levels between 2 and 5 percent RMS, when comparing the time response to the uncompensated time response. Multiple piezoelectric absorbers were implemented on the tool holder to improve the attenuation results of the cutting process by increasing the effective bandwidth of attenuation.

However the absorbers influenced each other and only 8.76 percent attenuation was obtained. A point inertance was measured at the tool tip to verify the influence of the piezoelectric absorber on the tool holder experimentally. Unfortunately, the influence of the piezoelectric absorber could not be verified experimentally during the cutting process, since no measurements could be made with 5 percent repeatability.

Shunted piezoelectric stack actuators can attenuate machine tool vibration. However, further development is required to improve the attenuation performance during the machining operation, in order to make the concept feasible.

6.2 Recommendations for future research

6.2.1 FEM of the machine tool structure

The accuracy of the finite element model must be improved to enable the development of a design procedure for optimal support structures. The complex interaction of the systems bolted connections is an area of concern and new innovative ideas are required to model the connections.

6.2.2 Multiple resonant shunt circuits

Browning and Wynn [10] developed a wide band passive electronic shunt circuit with which they attenuated twelve modes of a plate structure. It might be possible to manipulate the FRF at the tool tip with such a wide band shunt circuit to improve the attenuation results during the machining process.

6.2.3 Leverage implementation on the piezoelectric absorber

A number of machining operations was performed during the attempts to quantify the influence of the piezoelectric absorber on the tool tip. During the different operations no significant change in the shunt resistor's temperature was observed. The observation raises the question on whether the piezoelectric damper is optimally utilised. The amount of strain applied by the displacement of the tool holder might not be enough to fully utilise the energy capturing ability of the piezoelectric stack actuator. The addition of a leverage system might improve the utilisation of the shunted piezoelectric actuator's energy capturing ability.

6.2.4 Behaviour of the piezoelectric absorber under load conditions

The model developed in the research is merely a linear approximation of the passively shunted piezoelectric actuator's behaviour. The true behaviour of the system under load conditions and the boundaries of the linear approximation are unknown. The behaviour has to be determined before an effective leverage system can be designed.